The Astrophysical Journal, 771:109 (7pp), 2013 July 10 doi:10.1088/0004-637X/771/2/109


# SEARCH FOR RAYLEIGH SCATTERING IN THE ATMOSPHERE OF GJ1214b

E. J. W. de Mooij[1], M. Brogi[2], R. J. de Kok[3], I. A. G. Snellen[2], B. Croll[4,5], R. Jayawardhana[1], H. Hoekstra[2], G. P. P. L. Otten[2], D. H. Bekkers[2], S. Y. Haffert[2], and J. J. van Houdt[2]
[1] Department of Astronomy and Astrophysics, University of Toronto, 50 St. George Street, Toronto, ON M5S 3H4, Canada; demooij@astro.utoronto.ca
[2] Leiden Observatory, Leiden University, Postbus 9513, 2300-RA, Leiden, The Netherlands
[3] SRON Netherlands Institute for Space Research, Sorbonnelaan 2, 3584-CA, Utrecht, The Netherlands
[4] Kavli Institute for Astrophysics and Space Research, Massachusetts Institute of Technology, Cambridge, MA 02139, USA
*Received 2013 March 11; accepted 2013 May 17; published 2013 June 24*

## ABSTRACT

We investigate the atmosphere of GJ1214b, a transiting super-Earth planet with a low mean density, by measuring its transit depth as a function of wavelength in the blue optical portion of the spectrum. It is thought that this planet is either a mini-Neptune, consisting of a rocky core with a thick, hydrogen-rich atmosphere, or a planet with a composition dominated by water. Most observations favor a water-dominated atmosphere with a small scale-height, however, some observations indicate that GJ1214b could have an extended atmosphere with a cloud layer muting the molecular features. In an atmosphere with a large scale-height, Rayleigh scattering at blue wavelengths is likely to cause a measurable increase in the apparent size of the planet toward the blue. We observed the transit of GJ1214b in the *B* band with the FOcal Reducing Spectrograph at the Very Large Telescope and in the *g* band with both ACAM on the William Herschel Telescope (WHT) and the Wide Field Camera at the Isaac Newton Telescope (INT). We find a planet-to-star radius ratio in the *B* band of $0.1162 \pm 0.0017$, and in the *g* band $0.1180 \pm 0.0009$ and $0.1174 \pm 0.0017$ for the WHT and INT observations, respectively. These optical data do not show significant deviations from previous measurements at longer wavelengths. In fact, a flat transmission spectrum across all wavelengths best describes the combined observations. When atmospheric models are considered, a small scale-height water-dominated model fits the data best.

*Key words:* planetary systems – stars: individual (GJ1214) – techniques: photometric

*Online-only material:* color figures

## 1. INTRODUCTION

The transiting planet GJ1214b (Charbonneau et al. 2009) is currently the best studied super-Earth. With a radius of 2.6 $R_{\rm Earth}$ and a mass of 6.5 $M_{\rm Earth}$, its density is significantly lower than that of the Earth. Rogers & Seager (2010) explain the low density of GJ1214b in the context of three different formation models; two of these models result in a thick atmosphere with a low mean-molecular weight and a large scale-height, while the third scenario, that GJ1214 is a water world, predicts a small scale-height due to the large mean-molecular weight of water compared to hydrogen.

Models for GJ1214b's atmosphere showed that in the case of a hydrogen-rich atmosphere, signatures of the atmosphere should be well within the reach of current instrumentation (Miller-Ricci & Fortney 2010; Howe & Burrows 2012). Many observations probing the atmosphere of GJ1214 have been presented in the literature (Bean et al. 2010, 2011; Croll et al. 2011; Crossfield et al. 2011; Berta et al. 2012; de Mooij et al. 2012; Murgas et al. 2012; Narita et al. 2013; Fraine et al. 2013; Teske et al. 2013). Although most of these observations did not show the expected features of an extended atmosphere, Croll et al. (2011) found an increased radius in the *K* band indicative of molecular absorption, and (de Mooij et al. 2012, hereafter Paper I) reported a tentative signal from Rayleigh scattering toward blue wavelengths. In the case that the atmosphere of GJ1214b is extended, the lack of spectral features at longer wavelengths can be explained by a low abundance of methane, as well as a cloud layer that masks the features.

[5] NASA Sagan Fellow.

Here, we present the results of transit observations at blue optical wavelengths in order to investigate the tentative signal of Rayleigh scattering found in Paper I. In Section 2, we report the observations. In Section 3, we describe the data reduction, corrections for systematic effects, and the transit fitting. In Section 4, we discuss our results in the context of atmospheric models. Finally, we present our conclusions in Section 5.

## 2. OBSERVATIONS

### 2.1. Transit Observations with ACAM

On the night of 2011 May 22, a transit of GJ1214b was observed in the *g* band ($\lambda_c = 4996$ Å) with ACAM (Benn et al. 2008) on the William Herschel Telescope (WHT). The observations started at 23:59 UT and lasted for ~4.4 hr. An exposure time of 30 s was used, resulting in a total of 364 frames, with an average cadence of 44 s. The circular field of view of ACAM is 8 arcmin in diameter, allowing the observation of several reference stars simultaneously with the target. Due to the relative faintness of GJ1214 in the *g* band, we did not defocus the telescope. Despite guiding, flexing between the instrument and the guider resulted in a drift of 10 pixels (2.″5) during the night. Toward the end of the night, the sky became non-photometric, with an extinction of up to 20%, while the median seeing was 1.″2 (see Figure 1).

### 2.2. Transit Observations with FORS

A second transit of GJ1214 was observed with the FOcal Reducing Spectrograph (FORS) on the Very Large Telescope (VLT) on 2011 July 12 in the *B*-high filter ($\lambda_c = 4543$ Å). The observations, which lasted for $2^{\rm h}40^{\rm m}$, started at 01:28 UT.

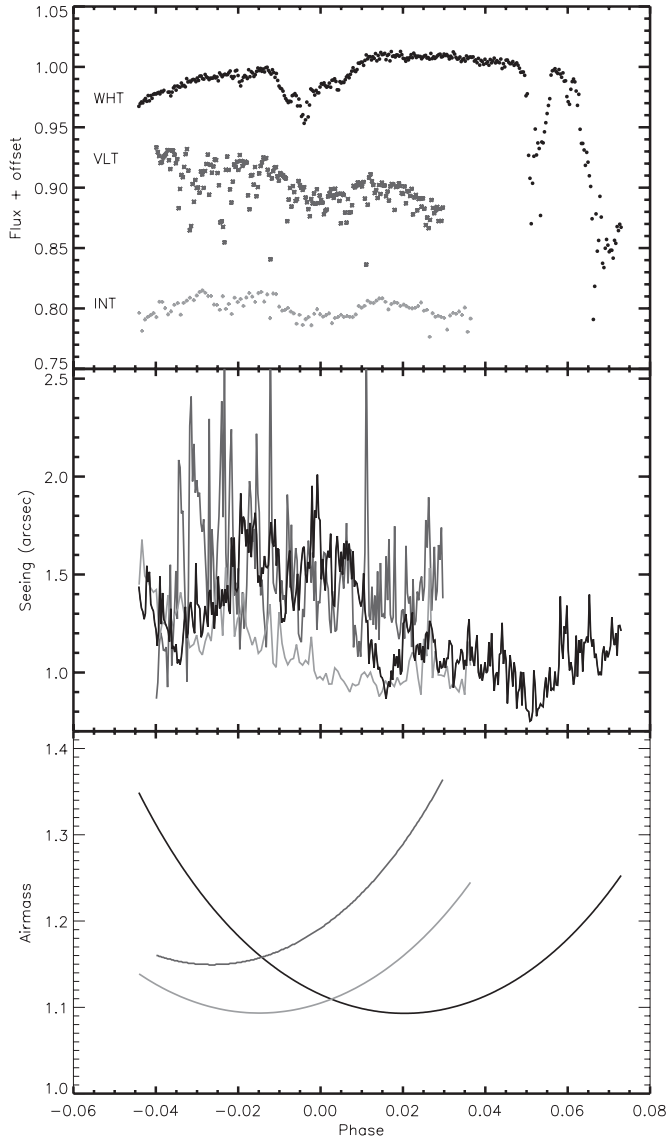


**Figure 1.** Top panel: light curves of GJ1214 without the use of a reference star for the three nights of observation. Middle panel: the seeing during the three nights; the WHT, VLT, and INT observations are shown with black, dark gray, and light gray lines, respectively. Bottom panel: the geometric air mass for the three transit observations.

A total of 205 frames with an exposure time of 20 s were obtained with an average cadence of 47 s. As with the WHT observations, the telescope was not defocused. To increase the cadence, the $2 \times 2$ binning mode was used, yielding a pixel scale of $0\farcs25$ pixel$^{-1}$. Although FORS consists of two detectors, only data from one detector were used, due to a systematic difference in the photometry between the detectors. The detector used has an unvignetted field of view of $7' \times 4'$. The seeing during the observations was highly variable, varying between $1''$ and $3''$ with a median of $1\farcs4$ (see Figure 1).

### 2.3. Transit Observations with WFC

On the night of 2012 May 6, a transit of GJ1214b was observed in the $g$ band ($\lambda_c = 4962$ Å) with the Wide Field Camera (WFC) of the Isaac Newton Telescope (INT). The observations lasted 3 hr and started at 02:35 UT. During this time, 113 frames were obtained with an average cadence of 97 s and an exposure time of 60 s. Although the camera consists of four CCDs, each with a pixel scale of $0\farcs33$ pixel$^{-1}$, only the central CCD (CCD4) was used, with a field of view of $\sim 22\farcm7 \times 11\farcm4$. The telescope was not defocused for these observations. The atmosphere was stable during the observations, and the median seeing was $1\farcs4$ (see Figure 1).

## 3. DATA REDUCTION AND ANALYSIS

The data from all telescopes were reduced in similar ways: after bias subtraction, the data were flat-fielded using a flat field created from twilight flats. The atmospheric dispersion corrector of the FORS instrument is known to introduce rotator angle dependent variations in the flat field (Moehler et al. 2010). Therefore, flat fields for the $B_{\rm high}$ filter at different rotator angles were obtained from the ESO archive for the period surrounding our observations. These flat fields were combined into a single master flat.

Subsequently, aperture photometry was performed on GJ1214 and a set of reference stars. Aperture radii of 18, 13, and 13 pixels were used for the ACAM, FORS, and WFC observations, respectively (4.5, 3.75, and 4.3 arcsec). These apertures were chosen to minimize the noise in the respective light curves. The photometry from multiple reference stars was combined into a master reference light curve for each of the observations. For the INT observations 13 reference stars were used, while the limited field of view for the other instruments limited the number of useable reference stars to 4 and 3 for the WHT and VLT, respectively. Although there are more stars inside the field of view, many of them are either saturated or show strong systematic effects (for the VLT, this might be due to the rotator angle dependence of the flat field). Subsequently, the light curve for GJ1214 was divided by the master reference light curve and normalized.

### 3.1. Light-curve Fitting

The normalized light curves are shown in Figure 2. No strong systematic effects are seen in the WHT and INT light curves, while the VLT light curve shows a smooth gradient. We fit this trend simultaneously with the transit depth using a Markov Chain Monte Carlo (MCMC) method. The transit is modeled using the Mandel & Agol (2002) routines with the scaled semimajor axis and the impact parameters fixed to those from Bean et al. (2010; $a/R_* = 14.9749$ and $b = 0.2779$); the limb darkening was also kept fixed, to the values from Claret (2000) for the VLT observations, while for the WHT and INT observations limb-darkening coefficients from Claret (2004) were used. We used the quadratic limb-darkening coefficients for a star with $T_{\rm eff} = 3030$ K and $\log(g) = 5.0$. The time of mid-transit and the planet-to-star radius ratio are free parameters. We verified that when we include the impact parameter, semimajor axis, and limb darkening as free parameters, we obtain consistent results.

Three different models were used to correct the systematic effects in the baseline: a model depending on the geometric air mass, a second-order polynomial baseline model, and a third-order polynomial baseline model. For each combination of light curve and baseline model, we created five separate MCMC chains of 200,000 steps for which the first 20,000 steps were discarded to remove the burn-in. Subsequently, these five chains were merged, after verifying that they had converged using the Gelman–Rubin statistic (Gelman & Rubin 1992). The results of these MCMC chains are given in Table 1.

The impact of red noise was assessed using the residual permutation (Prayer-bead) method (e.g., Gillon et al. 2007) for

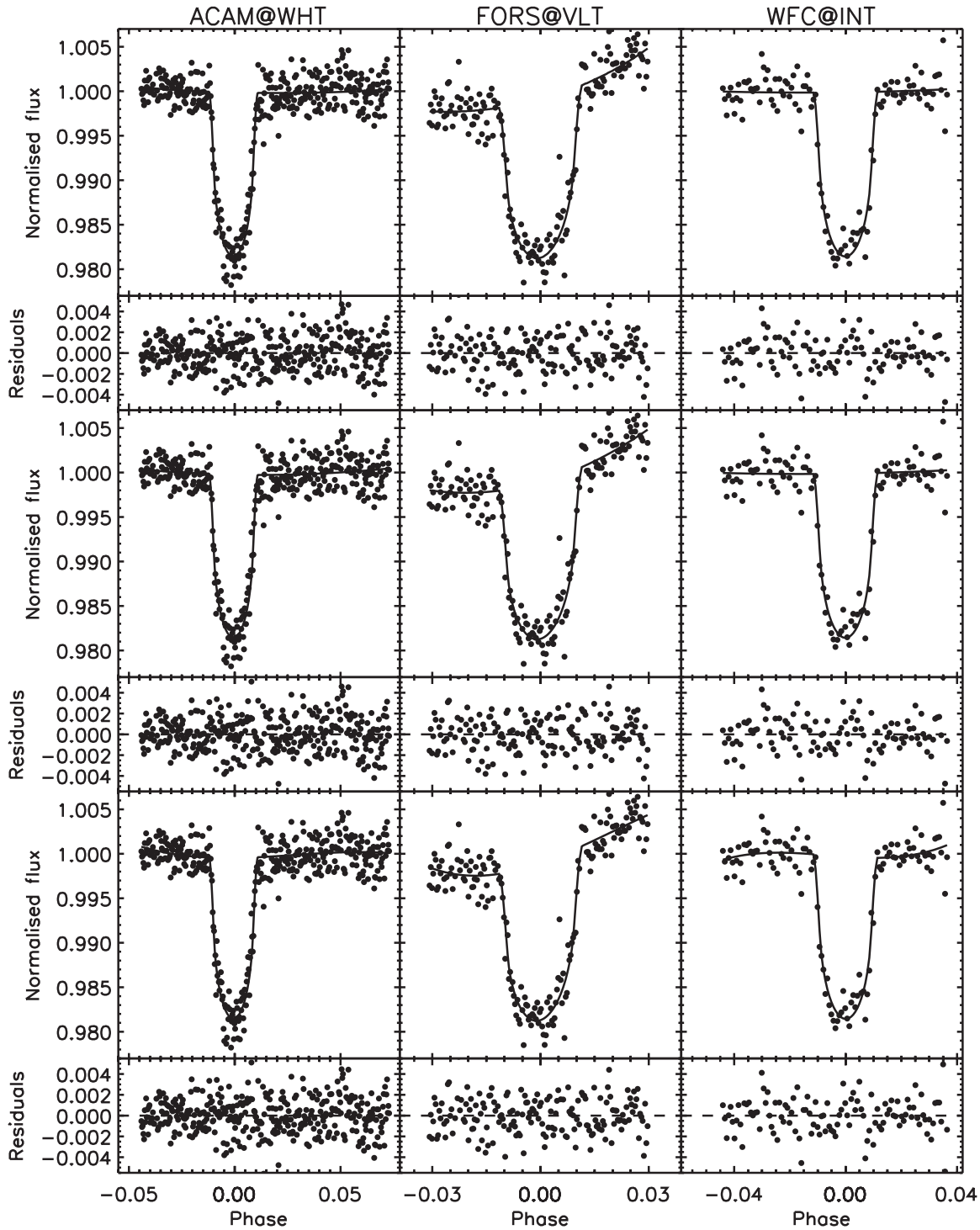


**Figure 2.** Light curves and residuals for the WHT (left panels), VLT (middle panels), and INT (right panels) data sets. Overplotted are the best-fitting models for a baseline based on air mass (first two rows), second-order polynomial (middle two rows), and third-order polynomial (bottom two rows).

**Table 1**
Measurements of $R_p/R_*$ for the Three Observations and Different Baseline Models

| Baseline | WHT $g$ band | VLT $B$ band | INT $g$ band |
|---|---|---|---|
| Air mass | $0.1180 \pm 0.0009$ | $0.1168 \pm 0.0012$ | $0.1181 \pm 0.0014$ |
| Second order | $0.1176 \pm 0.0010$ | $0.1161 \pm 0.0017$ | $0.1181 \pm 0.0017$ |
| Third order | $0.1168 \pm 0.0011$ | $0.1163 \pm 0.0017$ | $0.1174 \pm 0.0017$ |

each of the data sets. The 16% and 84% distributions of the fitted parameters are taken as the $\pm 1\sigma$ confidence interval. The radius ratios with uncertainties as determined from this analysis are given in Table 2. As can be seen, the uncertainties from this analysis indicate that the contribution from red noise is small. We therefore adopt the measurements from the MCMC analysis for the rest of this work.

As an additional check on the robustness of the fit, we determined the radius ratio for light curves generated using individual reference stars. In Figure 3, we show for each of the

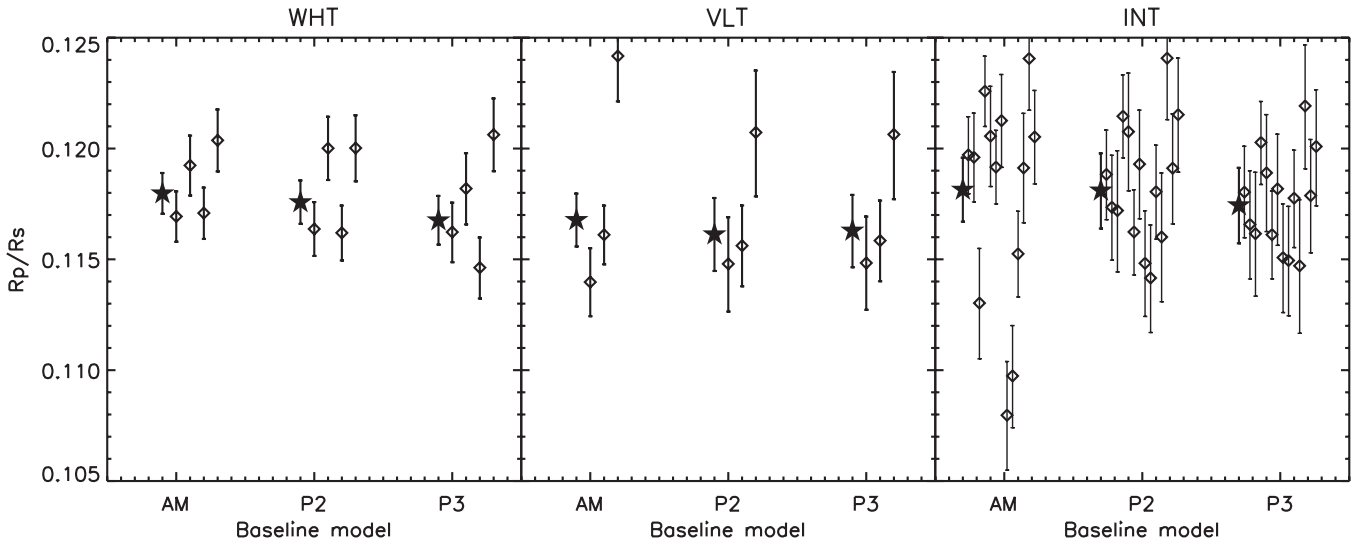


**Figure 3.** Measured planet-to-star radius ratios for the three data sets using three different baseline corrections. The filled stars are the values determined for the master light curve (the light curve of the target divided by the combined light curve of the reference stars), while the open diamonds are the radius ratios as determined when the light curve of the target is correct with the individual reference stars. The three different baselines are: air mass (AM), second-order polynomial (P2), and third-order polynomial (P3).

**Table 2**
Measurements of $R_p/R_*$ for the Three Observations and Different Baseline Models from the Residual Permutation (Prayer-bead) Method

| Baseline | WHT $g$ band | VLT $B$ band | INT $g$ band |
|---|---|---|---|
| Air mass | $0.1181^{+0.0005}_{-0.0010}$ | $0.1165^{+0.0010}_{-0.0003}$ | $0.1180^{+0.0008}_{-0.0009}$ |
| Second order | $0.1174^{+0.0006}_{-0.0009}$ | $0.1160^{+0.0006}_{-0.0003}$ | $0.1180^{+0.0008}_{-0.0009}$ |
| Third order | $0.1165^{+0.0006}_{-0.0007}$ | $0.1162^{+0.0002}_{-0.0003}$ | $0.1172^{+0.0009}_{-0.0008}$ |

**Note.** The quoted $R_p/R_*$ is for the median of the distribution, and the upper and lower uncertainties are for the 16% and 84% levels, respectively.

three data sets the measured radius ratios for both a reference signal based on an ensemble of light curves and for the individual light curves. As can be seen, most of the measurements for the individual stars agree well with the measurement for the combined reference signal, except for the air mass baseline fit to the INT $g$-band data. For the rest of the paper we adopt the baseline with air mass only for the WHT observations, the results for the second-order polynomial for the VLT observations, and the model with the third-order polynomial baseline for the INT observations. The rms of the residuals of the data with the selected baselines are 1.68 mmag, 1.89 mmag, and 1.66 mmag for the WHT, VLT, and INT data, respectively.

## 4. RESULTS AND DISCUSSION

We find planet-to-star radius ratios of 0.1180 ± 0.0009, 0.1162 ± 0.0017, and 0.1174 ± 0.0017, respectively, for the WHT $g$ band, the VLT $B$ band, and the INT $g$ band. These radii are consistent with radius ratios measured at a longer wavelength (e.g., from the MEarth data; Charbonneau et al. 2009), and do not confirm the potential $2\sigma$ deviation in the $g$ band found in Paper I. In addition to the data above, GJ1214b has been observed by many other groups, and the available data from the literature span wavelengths from ∼0.4 $\mu$m to ∼5 $\mu$m (Bean et al. 2010, 2011; Désert et al. 2011; Croll et al. 2011; Berta et al. 2012; Narita et al. 2013; Fraine et al. 2013; Teske et al. 2013, Paper I). Although most of these data sets use the same parameters for the system (from Bean et al. 2010), some (e.g., Berta et al. 2011) use a different set of parameters, which could cause an offset, making a direct comparison between the measured radius ratios more difficult. In addition, we note that GJ1214 is an active star and that the presence of starspots could bias the measurement of the radius measurements (see Section 4.3). Since the measurements from the literature were made at different dates, and therefore different levels of stellar activity, this could influence the observed transmission spectrum. In Figure 4, we show the transmission spectrum of GJ1214b based on our measurements and those from the literature listed above.[6]

### 4.1. Comparison with Atmospheric Models

We compared the observed wavelength-dependent transmission spectrum with a set of models for three different scenarios for the nature of the atmosphere of GJ1214: an atmosphere with a small scale-height (a "water world"), a large scale-height atmosphere without clouds, and an atmosphere with clouds and a large scale-height. The models are the same as used in Paper I.

We have overplotted the models on the data in Figures 4 and 5. As can be seen, the model with the large scale-height and no clouds (green dash-dotted line) can clearly be excluded. The water-world model (blue, dashed-triple dotted line) and the model with a large scale-height and a cloud layer (red dashed line) are both consistent with the data.

Assuming that all the uncertainties on the measurements are reliable, we can calculate the formal $\chi^2$ for each of the three models. For the water world $\chi^2 = 190$, for the cloudless atmosphere $\chi^2 = 4003$, and for the atmosphere with clouds $\chi^2 = 289$, while a flat line gives $\chi^2 = 148$. From this it follows that the current available data favor a flat transmission spectrum (i.e., no atmosphere or a gray atmosphere), followed by a water-dominated atmosphere. In this paper, a total of 92 measurements of the radius are used. Note that assigning degrees of freedom to each of these models is not very useful, since there are many different parameters that can be adjusted (e.g., composition and temperature–pressure profile).

[6] Note that in the case of papers with multiple measurements with the same wavelength and instrument, we use the value for the combined fit to the data.

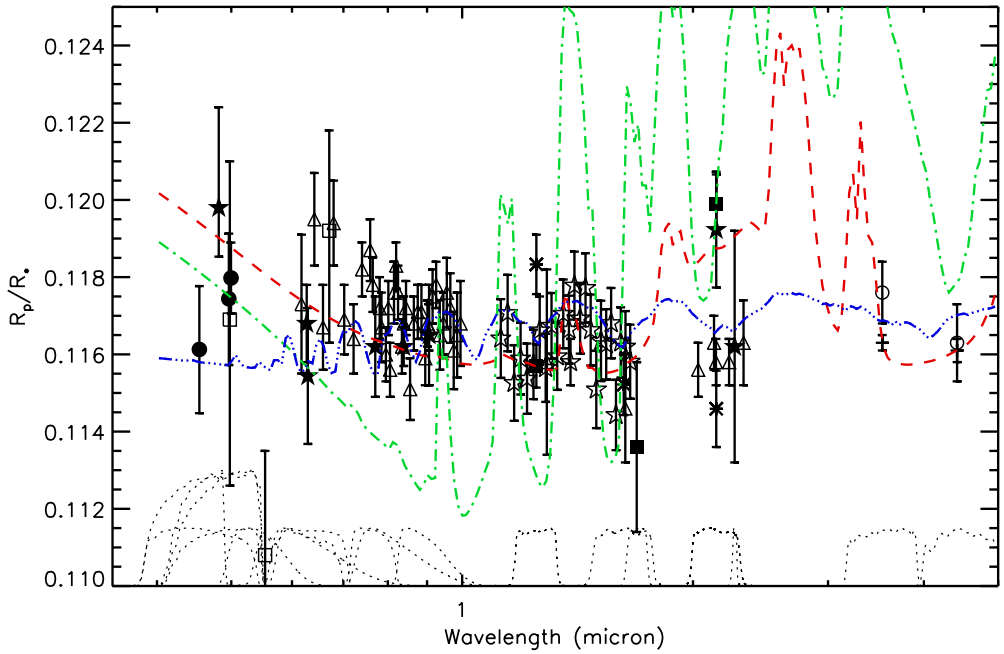


**Figure 4.** Transmission spectrum of GJ1214b, including all available measurements from the literature. The filled circles are the observations from this work, the filled stars are for data from Paper I, the filled squares are for data from Croll et al. (2011), the open triangles are for data from Bean et al. (2011), the open stars are for data from Berta et al. (2012), the open circles are for data from Désert et al. (2011), the asterisks are for data from Narita et al. (2013), the crosses are for data from Fraine et al. (2013), and the open squares are for data from Teske et al. (2013). Overplotted are the three models for the atmosphere of GJ1214b: a hydrogen-dominated atmosphere with solar composition (green line), a hydrogen-dominated atmosphere with clouds and low methane abundance (red line), and a water-dominated atmosphere (blue line). The dashed curves at the bottom are the transmission curves for the different filters. Note that for clarity, the filter curves for the data from Bean et al. (2011) and Berta et al. (2012) have been omitted since they are effectively flat.

(A color version of this figure is available in the online journal.)

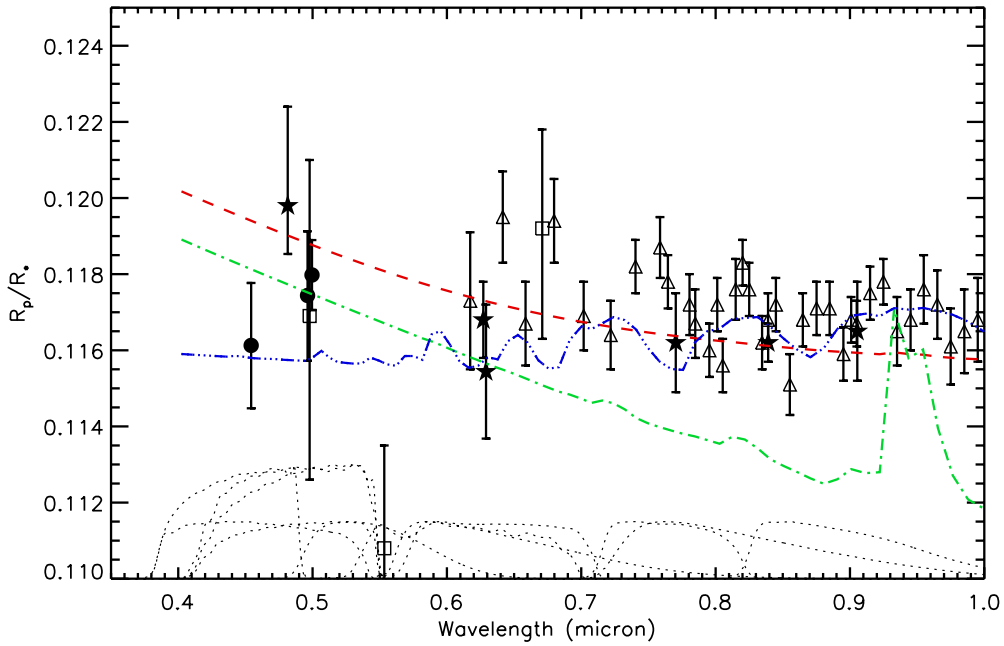


**Figure 5.** Same as Figure 4 but now only focusing on the optical part of the spectrum.

(A color version of this figure is available in the online journal.)

### *4.2. Potential Origins of a Flat Transmission Spectrum*

As discussed above, and by various other authors, the best fit to the collective set of measurements of the transit depth is a flat line. Here we briefly discuss some physical possibilities that can create such a flat transmission spectrum. Although unlikely, a flat transmission spectrum could indicate that GJ1214b lacks an atmosphere with the density of the planet, which requires either a water-dominated planet or a planet with an extended envelope (Rogers & Seager 2010).

In the case of an extended atmosphere, the presence of clouds can also result in a gray transmission spectrum. This point is mentioned by several authors in a qualitative manner (e.g., Bean et al. 2010; de Mooij et al. 2012; Howe & Burrows 2012), but

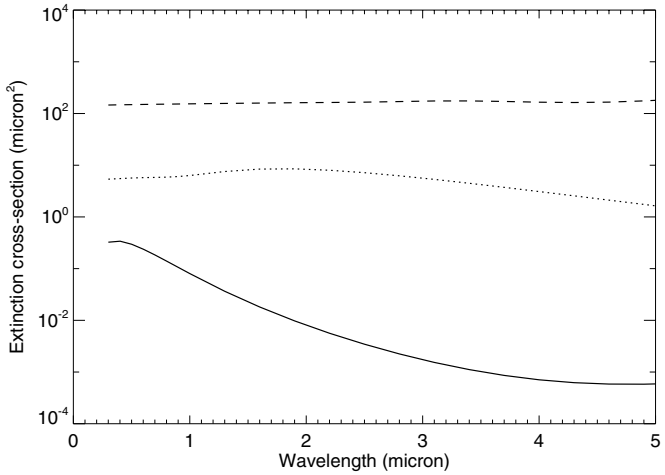


**Figure 6.** Extinction cross-section for $Mg_2SiO_4$ particles with narrow log-normal size distributions around 5.0, 1.0, and 0.2 $\mu$m, respectively, from top to bottom.

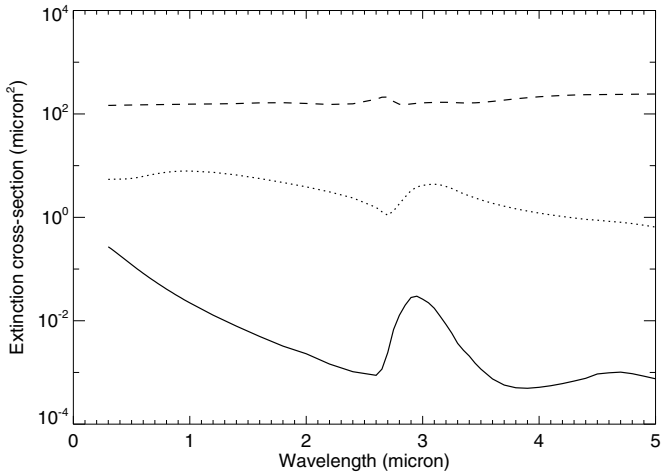


**Figure 7.** Extinction cross-section for $H_2O$ droplets with narrow log-normal size distributions around 5.0, 1.0, and 0.2 $\mu$m, respectively, from top to bottom.

it needs pointing out that such a cloud would have to meet specific requirements to produce a flat spectrum (see also Berta et al. 2012). One option is that there is an optically thick cloud, which itself has a wavelength-independent extinction, at high enough altitudes to cover any gas absorption features. Such a cloud can be vertically extended, as long as it is optically thick when seen in transmission. Because of the wavelength-independent extinction, the altitude at which the cloud becomes optically thick will also be independent of wavelength. For cloud properties to be constant with wavelength, the particles need to be larger in size than the wavelength range. Figure 6 shows an example of the extinction cross-sections as a function of wavelength for $Mg_2SiO_4$ particles, which has only slowly varying optical constants along these wavelengths and is not strongly absorbing. On the other hand, Figure 7 shows the extinction cross-sections for the same particle size distributions for water droplets, which has a clear absorption feature around 3 $\mu$m. Even for the large particles, the extinction cross-section is significantly larger there than at other wavelengths. For both $Mg_2SiO_4$ and $H_2O$, the cross-sections are calculated using a Mie code based on de Rooij & van der Stap (1984).

Alternatively, if the clouds have a very sharp decrease of optical depth above the cloud tops, then that could also result in a featureless transmission spectrum. If the cloud is optically thick

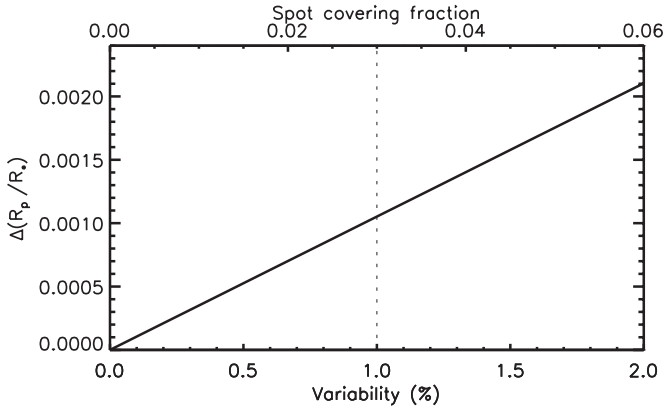


**Figure 8.** Change in $R_p/R_*$ in the $g$ band as a function of stellar variability in the $I$ band. The corresponding spot coverage fraction, assuming a spot temperature of 2800 K, is indicated above. The stellar variability as measured by Berta et al. (2011) is ∼1% in the MEarth bandpass, comparable to the $I$ band used here, and is indicated by a dashed line.

along the slant path through the atmosphere, then variations of cloud properties with wavelength are irrelevant. The cloud then still needs to be above the altitude where gas absorption is important. Note that at present, we cannot constrain a pressure range of the cloud tops, since we do not know the gas abundances. For instance, Lammer et al. (2013) show that atmospheric escape can be very important for GJ1214b, which will change the composition of the atmosphere. The pressure limits mentioned by Berta et al. (2012) are only valid for a solar composition atmosphere in chemical equilibrium.

Finally, a sharp drop of gas volume mixing ratio, for instance, due to condensation, photolysis, or ionization (e.g., Miller-Ricci Kempton et al. 2012), can make a transmission spectrum appear flatter across all wavelengths, although this is unlikely to yield a perfectly flat transmission spectrum.

### *4.3. Stellar Variability*

In the discovery paper, Charbonneau et al. (2009) noted that the host star, GJ1214, is variable with a period of tens of days, which they attribute to starspots rotating in and out of view. Berta et al. (2011) used more measurements from MEarth and found an average variability of 1% on a period of ∼50 days. Unocculted starspots, whether contributing to the stellar variability or not, can, as discussed in Paper I (see also Sing et al. 2011; Désert et al. 2009), have a significant impact on the observed transmission spectrum. The WHT, INT, and VLT observations were taken over the span of approximately a year, and are, most likely, at different levels of stellar variability. This could lead to systematic differences in the measured radius ratios. Assuming a spot temperature of 2800 K (∼200 K lower than the temperature of the stellar photosphere), the ∼1% variability from Berta et al. (2011) corresponds to a bias in the radius ratio of ∼0.001 in the $g$ band (see Figure 8). Since we do not have contemporary measurements of the variability for all the observations, we do not correct our measurements for this effect.

As noted in Paper I, a background of unocculted starspots, which does not contribute to the stellar activity, could also significantly alter the shape of the transmission spectrum.

## 5. CONCLUSIONS

We have observed three transits of GJ1214b at blue optical wavelengths in order to search for the signature of Rayleigh scattering in its atmosphere, which should be present if its

atmosphere has a low mean-molecular weight and no large cloud particles. We find planet-to-star radius ratios of $0.1180 \pm 0.0009$, $0.1162 \pm 0.0017$, and $0.1174 \pm 0.0017$ in the $g_{\rm WHT}$, $B_{\rm high}$, and $g_{\rm INT}$ bands, respectively, and we do not confirm the potential $2\sigma$ signal of Rayleigh scattering presented in Paper I. Combining these measurements with values from the literature and comparing the full wavelength-dependent transmission spectrum with atmospheric models, we find that a model with a large scale height and no cloud layer is incompatible with the available data. Both a model with a large scale height and a cloud layer and a model for an atmosphere with a small scale-height are a better fit to the data with the water model favored over the model for an extended atmosphere with clouds. We therefore conclude that based on the currently available data, GJ1214b probably has an atmosphere with a small scale-height, although it should be noted that a featureless transmission spectrum provides the lowest $\chi^2$. This flat spectrum could be due to clouds, as discussed in Section 4.2.

We are grateful to the staff of the Isaac Newton Group, ESO's Paranal observatory. The Isaac Newton Telescope is operated on the island of La Palma by the Isaac Newton Group in the Spanish Observatorio del Roque de los Muchachos of the Instituto de Astrofísica de Canarias. This work is based on observations collected at the European Southern Observatory, Chile (287.C-5035). E.dM. is supported in part by an Ontario Postdoctoral Fellowship. This work is supported in large part by grants to R.J. from the Natural Sciences and Engineering Research Council of Canada, which also funds B.C.'s research. B.C.'s work was performed under a contract with the California Institute of Technology funded by NASA through the Sagan Fellowship Program.

## REFERENCES

Bean, J. L., Désert, J.-M., Kabath, P., et al. 2011, ApJ, 743, 92
Bean, J. L., Kempton, E., & Homeier, D. 2010, Natur, 468, 669
Benn, C., Dee, K., & Agócs, T. 2008, Proc. SPIE, 7014, 70146X
Berta, Z. K., Charbonneau, D., Bean, J., et al. 2011, ApJ, 736, 12
Berta, Z. K., Charbonneau, D., Désert, J.-M., et al. 2012, ApJ, 747, 35
Charbonneau, D., Berta, Z. K., Irwin, J., et al. 2009, Natur, 462, 891
Claret, A. 2000, A&A, 363, 1081
Claret, A. 2004, A&A, 428, 1001
Croll, B., Albert, L., Jayawardhana, R., et al. 2011, ApJ, 736, 78
Crossfield, I. J. M., Barman, T., & Hansen, B. M. S. 2011, ApJ, 736, 132
de Mooij, E. J. W., Brogi, M., de Kok, R. J., et al. 2012, A&A, 538, A46
de Rooij, W. A., & van der Stap, C. C. A. H. 1984, A&A, 131, 237
Désert, J.-M., Bean, J., Miller-Ricci Kempton, E., et al. 2011, ApJL, 731, L40
Désert, J.-M., Lecavelier des Etangs, A., Hébrard, G., et al. 2009, ApJ, 699, 478
Fraine, J. D., Deming, D., Gillon, M., et al. 2013, ApJ, 765, 127
Gelman, A., & Rubin, D. B. 1992, StaSc, 7, 457
Gillon, M., Demory, B., Barman, T., et al. 2007, A&A, 471, L51
Howe, A. R., & Burrows, A. S. 2012, ApJ, 756, 176
Lammer, H., Erkaev, N. V., Odert, P., et al. 2013, MNRAS, 430, 1247
Mandel, K., & Agol, E. 2002, ApJL, 580, L171
Miller-Ricci, E., & Fortney, J. J. 2010, ApJL, 716, L74
Miller-Ricci Kempton, E., Zahnle, K., & Fortney, J. J. 2012, ApJ, 745, 3
Moehler, S., Freudling, W., Møller, P., et al. 2010, PASP, 122, 93
Murgas, F., Pallé, E., Cabrera-Lavers, A., et al. 2012, A&A, 544, A41
Narita, N., Nagayama, T., Suenaga, T., et al. 2013, PASJ, 65, 27
Rogers, L. A., & Seager, S. 2010, ApJ, 716, 1208
Sing, D. K., Pont, F., Aigrain, S., et al. 2011, MNRAS, 416, 1443
Teske, J. K., Turner, J. D., Mueller, M., & Griffith, C. A. 2013, MNRAS, 431, 1669